PHOTOMASK

BACUS—The international technical group of SPIE dedicated to the advancement of photomask technology.

Best Oral Paper — PUV18

Design and implementation of the next generation electron beam resists for the production of EUVL photomasks

Scott M. Lewis, School of Chemistry and Photon Science Institute, The University of Manchester, Oxford Road, Manchester M13 9PL, United Kingdom; The Kavli Nanoscience Institute, California Institute of Technology, 1200 East California Boulevard, 107 – 81, Pasadena, CA USA

Hayden R. Alty, Christopher A. Muryn, Grigore A. Timco, Stephen G. Yeates, and Richard E. P. Winpenny, School of Chemistry and Photon Science Institute, The University of Manchester, Oxford Road, Manchester M13 9PL, United Kingdom

Guy A. DeRose, Matthew S. Hunt, Jarvis Li, Alex Werthiem, Trevor Fowler, Sang Kook Lee, and Axel Scherer, The Kavli Nanoscience Institute, California Institute of Technology, 1200 East California Boulevard, 107 – 81, Pasadena, CA USA 91125

ABSTRACT

A new class of resist materials has been developed that is based on a family of heterometallic rings. The work is founded on a Monte Carlo simulation that utilizes a secondary and Auger electron generation model to design resist materials for high resolution electron beam lithography. The resist reduces the scattering of incident electrons to obtain line structures that have a width of 15 nm on a 40 nm pitch. This comes at the expense of lowering the sensitivity of the resist, which results in the need for large exposure doses. Low sensitivity can be dramatically improved by incorporating appropriate functional alkene groups around the metal-organic core, for example by replacing the pivalate component with a methacrylate molecule. This increases the resist sensitivity by a factor of 22.6 and demonstrates strong agreement between the Monte Carlo simulation and the experimental results. After the exposure and development processes, what remains of the resist material is a metal-oxide that is extremely resistant to silicon dry etch conditions; the etch selectivity has been measured to be 61:1.

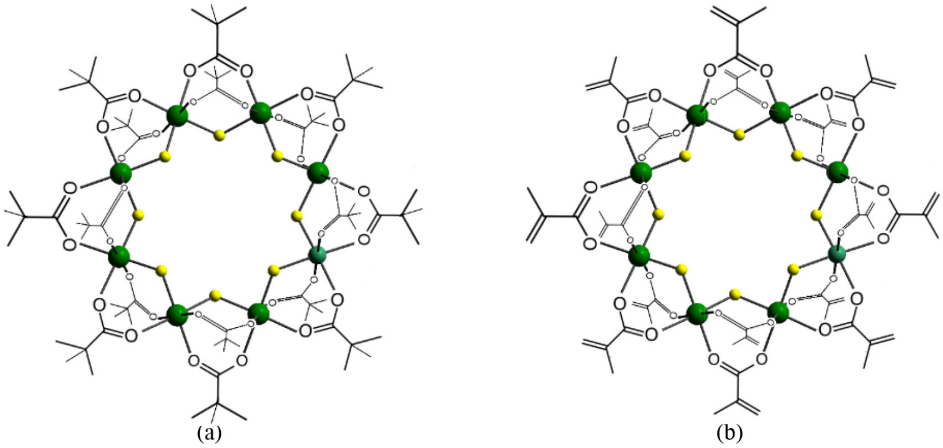

Figure 1. a) Cr_8F_8(Pivalate)16, b) Cr_8F_8(Methacrylate)$_{16}$. The structure of the molecules in a crystal, in ball-and-stick representation. Cr atoms are green and F atoms are yellow. H atoms are omitted for clarity.

BACUS NEWS

FEBRUARY 2019
VOLUME 35, ISSUE 2

TAKE A LOOK INSIDE:

SPIE.

10810-24

EDITORIAL

What Is the Modern BACUS?

Kent Nakagawa, Toppan Photomasks, Inc.

One of the very first conferences I attended in my professional career was the 1998 BACUS Photomask conference. And while it's very clear how much the photomask and semiconductor industry has changed since then (technology advances, business models, supplier/producer relationships, consolidation, etc.), there is much that has barely changed at all. Chrome-on-glass photomasks are still the volume leader and a key component even with leading-edge devices. Manufacturing equipment that are a generation older than my entry into the business are still in productive use. In a sense, the breadth of photomask manufacturing technology has grown along with our technological advancements that garner all the attention.

BACUS. For many of us veterans, it is synonymous with "the mask maker's conference". But what do those five letters actually mean? The title overhead on this newsletter says: "BACUS - The International technical group of SPIE dedicated to the advancement of photomask technology". There's a historical meaning. Its acronym comes from "Bay Area Chrome Users Society". And this is the first clear sign of how much has changed over the years. "Bay Area" - BACUS is a global society, no longer tied to its Silicon Valley roots. "Chrome" - we now process a variety of blanking materials for binary, phase-shift, and EUV, while chrome continues to be the primary workhorse.

It's the "Users" piece that I feel has seen the biggest change over the years. My first years were dominated by mask manufacturing participants - suppliers, equipment, and technology for mask manufacturing. These were the years just before the mass consolidation of suppliers and mask shops, followed by the birth of the foundries. My middle years saw the recognition of the photomask as a key imaging element, with OPC and PSM technologies. That brought in the EDA and wafer fab participants. In recent years, EUV has been the dominant topic. You can see this changing dialog as you browse through the conference session topics over the years.

How has our "Society" changed over the years? Unofficial SPIE data says that BACUS membership has declined by at least 2/3 since the mid 2000's. This suggest that maybe we haven't really changed enough from those early years? How will BACUS evolve for the next twenty years? Who are the "users" that the society represents. What should be the common concepts and drivers that will attract a fresh generation of engineers and companies to BACUS, and start reversing the membership decline? In short, what should a modern BACUS represent?

These are fundamental questions that need to be discussed not only by the BACUS steering committee, but by the BACUS membership at large. The semiconductor industry continues to evolve, and so must our own Society.

BACUS

N • E • W • S

BACUS News is published monthly by SPIE for BACUS, the international technical group of SPIE dedicated to the advancement of photomask technology.

Managing Editor/Graphics Linda DeLano
SPIE Sales Representative, Exhibitions, and Sponsorships Melissa Farlow
BACUS Technical Group Manager Marilyn Gorsuch

SPIE.

P.O. Box 10, Bellingham, WA 98227-0010 USA
Tel: +1 360 676 3290
Fax: +1 360 647 1445
SPIE.org
help@spie.org

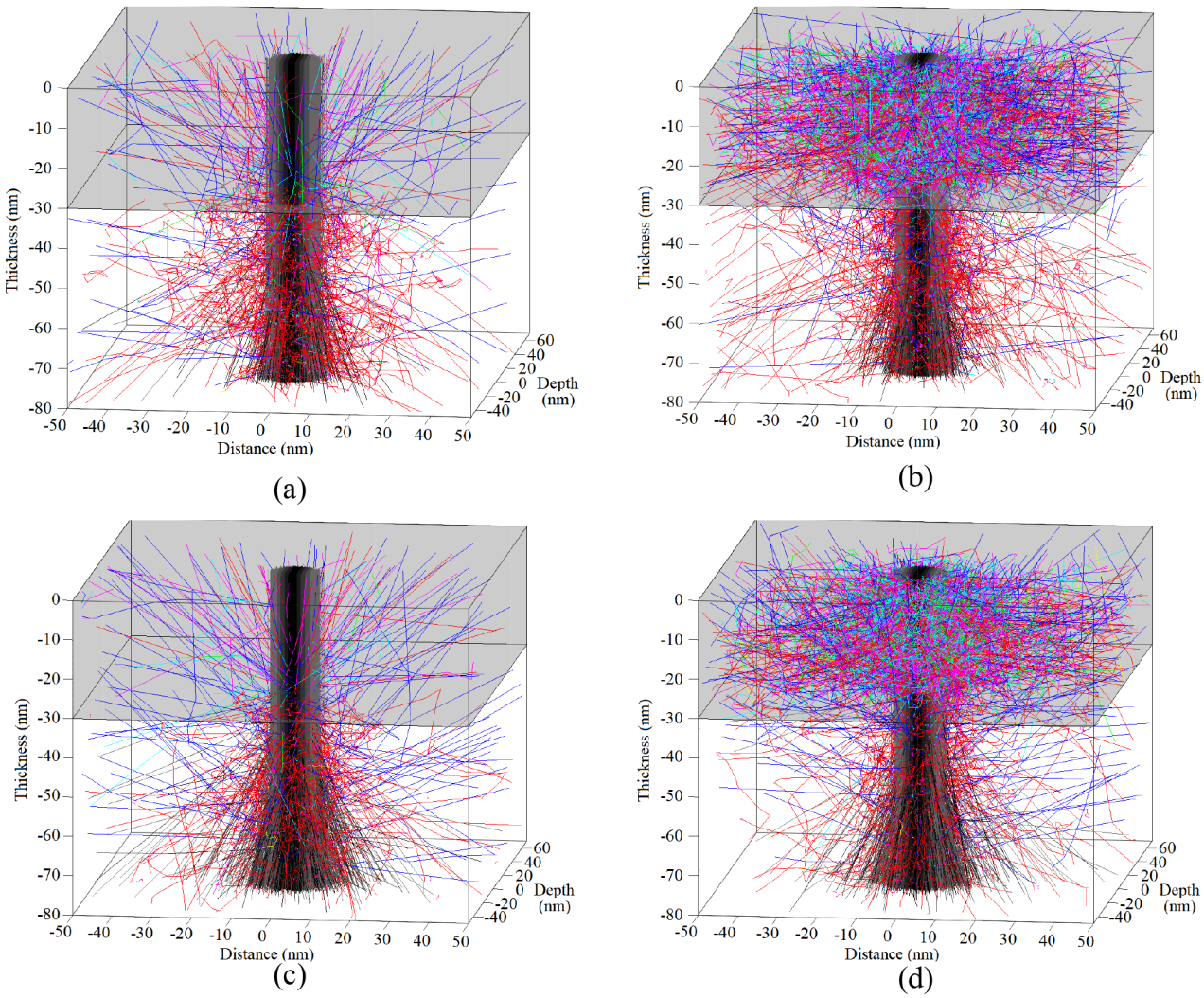

Figure 2. Point spread function of the internal electron scattering interactions inside (a) $Cr_8F_8(Pivalate)_{16}$ resist on 50 nm of Si. (b) $Cr_8F_8(Methacrylate)_{16}$ resist on 50 nm of Si, (c) $Cr_8F_8(Pivalate)_{16}$ resist on 50 nm of Cr, (d) $Cr_8F_8(Methacrylate)_{16}$ resist on 50 nm of Cr. The acceleration voltage used was 100 KeV. The black lines represent the PEs from the incident beam while the SEs above 500 eV are represented by the red lines. The SEs, which have associated energies below 500 eV, were generated by first, second and third order collisions and are indicated by purple, cyan and green, respectively. The blue lines are backscattered electrons. One million electrons are inserted into a single spot.

1. Introduction

The ability to write structures at the nanoscale using lithography underpins all modern, computer-based technology. The electronic devices we take for granted contain integrated circuits, the key component of which are field- effect transistors (FETs). These have reduced in size by a factor of two every two years over the past forty years, following "Moore's Law". The roadmap for the electronics industry now assumes that this constant reduction of size will continue, at least until the mid-2020s. Immersion 193 nm optical lithography (i193nm) is the current technique used to manufacture FinFETs, field-effect transistors with a shape resembling a fin. Unfortunately, this technique is reaching its physical limits in resolution. To counteract this, extreme ultra violet lithography (EUVL) has been promised to replace this technology. After two decades of outstanding research, numerous technical achievements, and multi-billion dollar investment, EUVL technology has only recently arrived into the research element of the semiconductor industry. While EUVL tools are being delivered, there is still a great need to develop new resist materials that will result in the creation of suitable EUVL photomasks. To achieve the 7 nm node that is expected to be in production by 2024, the features on the photomask, which are presently produced using electron beam lithography (EBL), are required to be 30 nm. Current e-beam resists cannot hit that specification, which means that new resists are needed in order to extract the full potential from EUVL.

Negative tone resists that are currently being used to fabricate photomasks for i193nm lithography are NEB22 (Sumitomo) and EVN30 (Shipley); they have a resolution of 40 and 50 nm, respectively[1, 2]. This resolution is required because the i193nm tools project the image onto photoresist and have lens reduction of 4x. Thus, to achieve the 14 nm node, features on the photomask need to be 56 nm. This is well outside the specification of 30 nm that is required for the production of EUVL photomasks. Another well-known issue presented by reducing feature sizes is that the required exposure dose to make them increases. This is leads to longer write times, thus decreasing the throughput of photomask creation. To alleviate this issue, new EBL tools that utilise

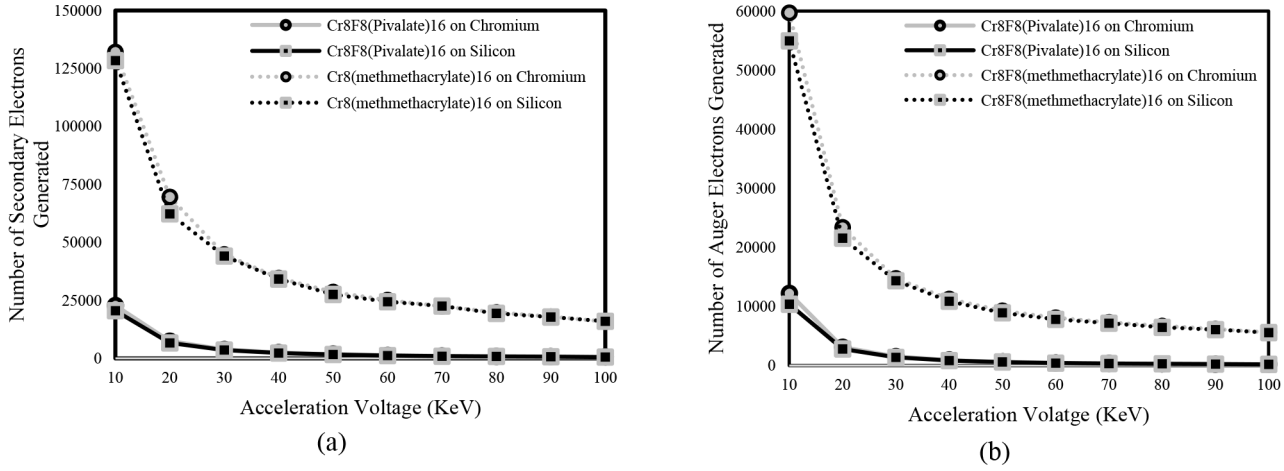

Figure 3. The number of Electrons generated in 30 nm thick resist films on 50 nm thick Si substrate. a) Total number of secondary electrons generated, b) Total number of Auger electrons generated from the resist materials.

Table 1. Physical properties of the resist materials and substrates.

Physical property	$Cr_8F_8(Pivalate)_{16}$	$Cr_8F_8(Methacrylate)_{16}$	Silicon	Chromium
Density (g/cm^3)	1.2	1.2	2.33	7.14
Effective Atomic Number	9.0	9.7	14	24
Average Atomic Weight (g/mol)	2192	3794	28.0855	51.9
Mean Ionization Potential (eV)	126.4	132.8	174	266.2

multiple beams are being designed to fabricate these photomasks. These tools have as many as 262,144 beams and have demonstrated a half-pitch resolution capability of 11 nm[3], but exposure times required for to exposure a full photomask are still too long. Therefore, new resist materials are required with higher sensitivities and higher resolution, and are the subject of this work.

Once the high-resolution pattern has been achieved, it must be transferred into the underlying substrate. This is usually achieved using an inductively-coupled plasma (ICP) etching technique. Etching nanostructures at dimensions that are less than 50 nm pitch, however, is very difficult because the probability of landing the neutral ions between features is extremely low[4]. This leads to a decrease in etch efficiency, which inherently decreases the etch rate and selectivity. To increase the etching efficiency, the ICP forward power can be increased, but this increases the etch rate of the resist, too, which would then require thicker resist to achieve the proper etch depth, which itself would require higher dose and result in reduced resolution. To avoid these interrelated issues, the ideal resist must be able to withstand the aggressive nature of the etching plasma. One method of achieving this is to incorporate metal materials into the resist. It has been shown that resists that are comprised of metal species exhibit small etch rates (because they have very little or no chemical reactivity with the gases that are used to etch the substrate) and consequently demonstrate large selectivities[4].

To address all of the above issues, we have developed a new class of resist materials that is based on a family of heterometallic rings[5]. Our resist material uses rigidity within the metal-organic molecule to achieve a very low density (ρ=1.212) while exhibiting a large molecular weight (2192 g/mol), which produces high resolution nanostructures. Figure 1a shows the resist molecule, established by the binding of eight chromium (Cr) atoms (in green) to form a ring-like frame structure; its chemical formula is $Cr_8F_8(C_5H_9O_2)_{16}$, denoted henceforth as $Cr_8F_8(Pivalate)_{16}$. The fabrication of this structure is described elsewhere[6]. The exterior of the compound, composed entirely of *tert*-butyl groups (pivalates), gives the compound high solubility in non-polar solvents and allows it to be spun onto substrates, e.g., silicon and chromium. Upon exposure to electrons, a bond scission interaction occurs, resulting in the carbon and oxygen atoms in the pivalate molecule reacting to form CO_2 gas, which volatilizes in the vacuum. This leaves behind a chromium oxide material that is insoluble in the developer solvent[4]. These resists write with very high resolution, but at the expense of lower sensitivity. To improve the resist sensitivity, we hypothesized that replacing the pivalate molecule with a methacrylate molecule (see Figure 1b) would lead to a reduction in the exposure dose without negatively impacting the resolution. The chemical formula of the resultant resist is $Cr_8F_8(C_4H_5O_2)_{16}$, denoted henceforth as $Cr_8F_8(Methacrylate)_{16}$. This resist has dangling alkene groups outside of the molecule that are free to activate a secondary electron (SE) generation mechanism when irradiated by incident lithography electrons. This results in more electrons scattering inside the resist, thus creating a chain reaction of cascading electrons that, upon each collision, exposes the resist in the immediate write area. This has the effect of increasing the overall sensitivity of the resist. It comes at the expense, of a large contribution to the proximity effect.

2. Simulation and Experimental

A Monte Carlo simulator was developed at the University of Manchester to gain a physical understanding of the internal electron scattering effects inside the $Cr_8F_8(Pivalate)_{16}$ and $Cr_8F_8(methacrylate)_{16}$ resist systems[4, 7]. Unfortunately, no single model accurately describes the electron behaviour in a resist for the energy range of 5 eV – 100 KeV. The simulator therefore uses two models to describe the electron scat-

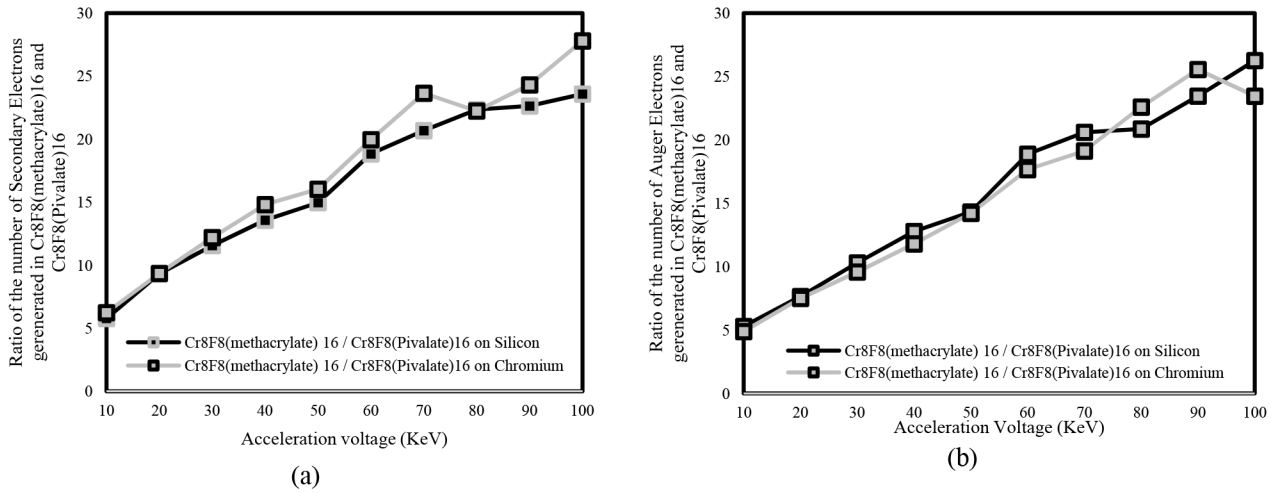

Figure 4. a) The ratio of secondary electrons generated by Cr_8F_8(Methacrylate)$_{16}$ and Cr_8F_8(Pivalate)$_{16}$ resists on 50 nm Si and Cr with varying acceleration voltage, b) The ratio of Auger electrons generated by Cr_8F_8(Methacrylate)$_{16}$ and Cr_8F_8(Pivalate)$_{16}$ resists on Siand Cr with varying acceleration voltage.

tering behaviour. The first utilizes the Joy model, which is based on Rutherford scattering and is an accepted estimate for electrons with kinetic energies above 500 eV, where quantum effects are ignored[8]. With each scattering event, the incident electron loses a portion of its initial energy and very often ends up with an energy below the 500 eV threshold. Therefore, a model for low-energy electrons (100eV and below) was also employed. This model uses the hard-sphere potential approximation, which exploits a quantum mechanical approach to electron scattering[9]. It incorporates the use of the partial wave expansion method (PWEM), which is a method for modelling low energy electrons scattering through metals and other solids[10 – 12].

It has been hypothesized that upon a collision event, both the primary electrons (PEs) and SEs experience the statistical chance of exhibiting the correct energy to emit an Auger electron (AE). Understanding the behaviour of these electrons is essential because they will be emitted from inner shells of the scattering atoms and will have a low energy that is suitable for generating even more SEs and AEs (this happens because the AE energy is lower than the first generation of AE emission, resulting in AE generation from the outer shells). Ultimately, this causes a cascading event as AEs travel through the immediate exposure area of the resist. These electrons contribute significantly to the proximity effect and therefore must be evaluated by the simulator. The Auger generation model is based on the work by Ding, which uses the Casnati cross-section for understanding inner shell ionization[13, 14].

The simulation was performed on a 30 nm layer of each electron beam resist, Cr_8F_8(Pivalate)$_{16}$ and Cr_8F_8(Methacrylate)$_{16}$, with an underlying 50 nm substrate of silicon and chromium, respectively. Table 1 shows the physical properties of each material. The incident electron beam had a Gaussian distribution of 3σ, where the spot size had a diameter of 2 nm. The simulation was run using 1,000,000 electrons to reduce the statistical error.

To fabricate a photomask, chromium is typically used as the absorbing photon layer. Therefore, the resist must be deposited on this material and patterned successfully by the EBL tool, followed by transfer of the high-resolution pattern into the Cr layer. In more detail, a 100 mm Si<100> wafer was coated with Cr using magnetron sputtering in an AJA Orion UHV series sputter system. The wafer process pressure was kept at 3 mtorr, as measured by a capacitance manometer utilizing downstream adaptive pressure control. Process gas species flow rates were kept constant at 20 sccm using a mass flow controller. The argon gas used for sputtering was of semiconductor grade purity. The thin film thickness and deposition rate data were measured by a quartz crystal thickness monitor. The system base pressure was 1E-8 torr prior to beginning deposition. The Cr layer was deposited with simultaneous RF substrate etching in order to smooth the RMS roughness. The substrate was pre-sputtered for 60 seconds at 100 W RF prior to the shutter opening. Deposition parameters included 200 W DC with a target power density of approximately 10 W/cm^2, to achieve a deposition rate of 1.22 Angstroms/s and an approximate thickness of 50 nm. The Cr layer was pre-sputtered for 60 seconds prior to shutter opening using the deposition parameters of 230 W DC with a target power density of approximately 10 W/cm^2, and a deposition rate of 0.58 Angstroms/s and an approximate thickness of 100 nm. The 100 W RF substrate etch was continued for the duration of the Chromium deposition and extended to account for back- sputtered material caused by the RF power delivered to the substrate. After the magnetron's shutter closed the RF power is ramped down over 40 seconds, resulting in some slight etching without any incoming Cr flux. The wafer was diced into 20 mm x 20 mm substrates.

The resist fabrication process is as follows. First, introduce 30 mg of Cr_8F_8(Pivalate)$_{16}$ to 3 g of Hexane and filter it using a 0.2 µm PTFE syringe filter. The Cr_8F_8(Pivalate)$_{16}$ resist was spun onto 20 mm x 20 mm silicon substrates. The resist was spun using a spin cycle of 6000 rpm for 40 seconds, which was followed by a soft bake at 100˚C for 2 minutes, allowing the cast solvent to evaporate. The resulting resist film had a thickness of 30 nm. This process was repeated for the Cr_8F_8(Methacrylate)$_{16}$ resist, except the hexane solvent was replaced with anisole. The Cr_8F_8(Pivalate)$_{16}$ resist was spun onto the Cr-coated silicon substrates using the same process that was used for coating the silicon substrates.

The exposure clearing dose of each resist material was determined from a one-dimensional matrix of a single pixel lines that were 5 µm long; the width of the line was the width of the electron beam, i.e. 2 nm. The one-dimensional matrix had each single pixel line separated by a pitch of 60, 55, 50, 45, and 40 nm. These were exposed with a dose range from 1000 to 80000 µC/cm^2 in incremental steps of 50 µC/cm^2. All resists were exposed using a Raith EPBG 5200 electron beam writer. The patterns were exposed using an acceleration voltage of 100 KeV, a probe current of 300 pA, and a step size of 5nm. The Cr_8F_8(Pivalate)$_{16}$ and Cr_8F_8(Methacrylate)$_{16}$ resists were developed in a bath of hexane and anisole, respectively, for 10 seconds. All samples were blown dry using Nitrogen (N_2).

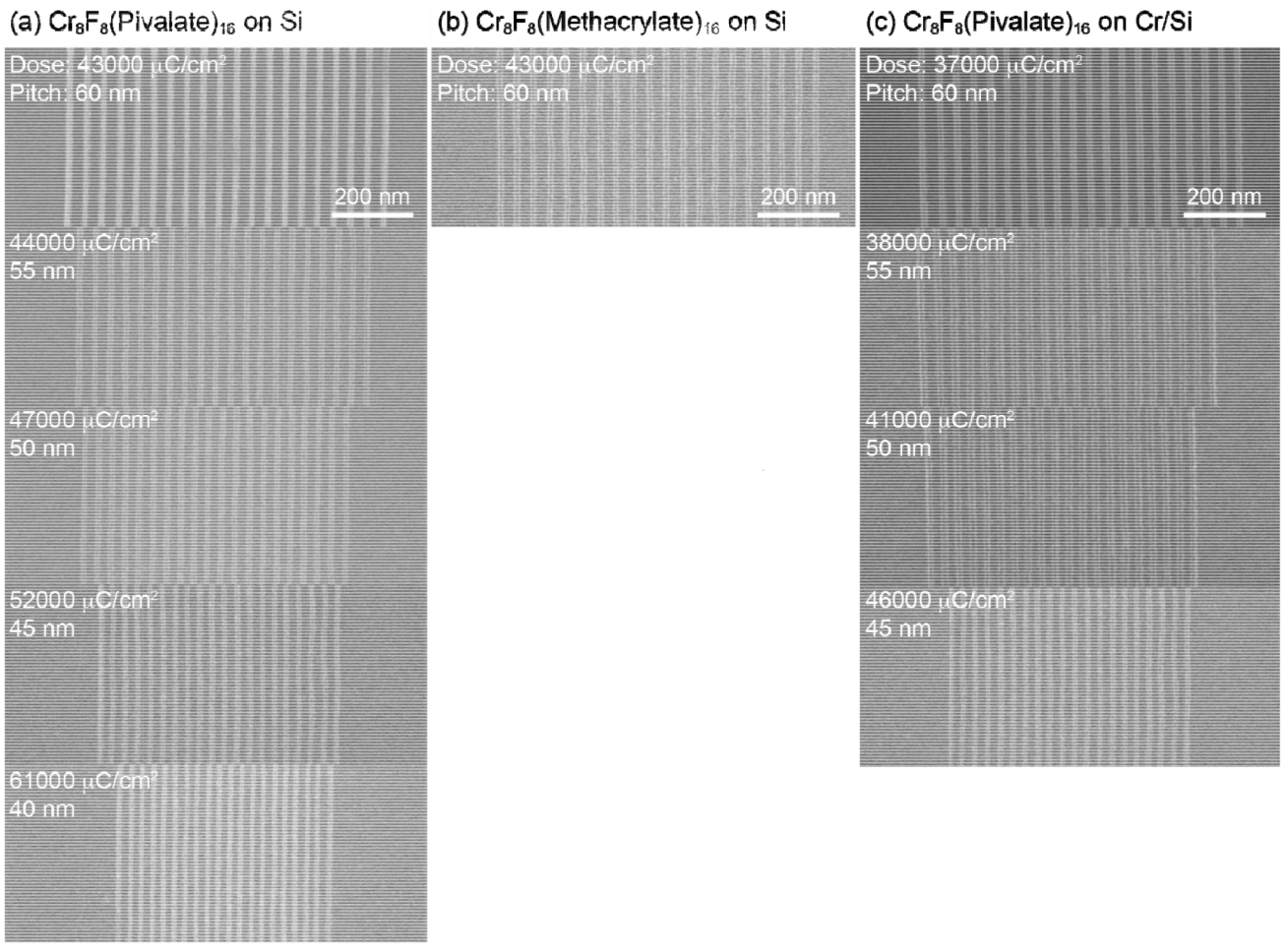

Figure 5. Effect of electron doses versus pitch on Si and Cr substrate materials. (a) Top down view of 15 nm lines on a 60, 55, 50, 45 and 40 nm pitch fabricated in Cr_8F_8(Pivalate)$_{16}$ resist on Si substrate. (b) Top down view of 15 nm lines on a 60 nm pitch fabricated in Cr_8F_8(methacrylate)$_{16}$ resist on Si substrate. (c) Top down view of 15 nm lines on a 60, 55, 50 nm pitch fabricated in Cr_8F_8(Pivalate)$_{16}$ resist on 100 nm of Cr on Si substrate.

3. Results and Discussion

Figure 2 shows a 3D scattering trajectory plot that illustrates that both of the resists confine the primary electrons (PEs) to within a 15 nm diameter of the immediate write area, suggesting that high resolution nanostructures would be expected. It is evident that Cr_8F_8(Methacrylate)$_{16}$ resist generates more SEs in the resist (see Figure 2b and d) than the Cr_8F_8(Pivalate)$_{16}$ resist (see Figure 2a and c).

This is important as these electrons are responsible for exposing the resist and subsequently increase the overall sensitivity while contributing to the proximity effect. When the methacrylate molecule is appended to the outside of the molecule, the dangling alkene groups are induced by the PEs to eject further SEs, which contribute to the reduction of the overall exposure dose. The associated energy of the SEs is considerably lower than that of the PEs, leading to an increased number of scattering events, with subsequent collisions generating even more SEs, thereby producing a cascade of scattering events. This effect can be seen in Figures 2b and d, where SEs are scattered at angles larger than 80° in arbitrary trajectories away from the primary beam, exposing the resist laterally. This is how the SE plays a major role in both widening the size of the nanostructure and producing a more sensitive resist.

Figure 3a shows the number of SEs generated inside each of the resists as a function of acceleration voltage. At the lower energies of 10 to 50 KeV, the PE is slow enough to cause multiple inelastic scattering events and generate more SEs, increasing the sensitivity of the resist while sacrificing resolution. At the higher energies of 50 to 100 KeV, the PEs have a lower probability of generating SEs and therefore more collisions are required in the resist material to lose sufficient energy and therefore to increase the probability of generating an SE (see Figure 2). As a consequence, a substantial number of incident electrons will come to rest deep in the Si substrate below without having participated significantly in exposing the resist, or otherwise can be backscattered into the underside of the resist material approximately 30-40 μm away from the immediate exposure area. Thus, while 100 KeV can achieve high resolution by narrowly confining the forward scattering of electrons inside the resist, this comes at the expense of higher dose and longer writing times. Currently, 50 KeV EBL tools are employed by the semiconductor industry because it best optimizes resolution versus writing time; Figure 3 reflects this philosophy.

It is clear that replacing the pivalate molecule with the methacrylate molecule significantly increases the number of SEs that are generated, thus predicting that the Cr_8F_8(Methacrylate)$_{16}$ resist will have increased sensitivity compared to Cr_8F_8(Pivalate)$_{16}$. This is due to the methacrylate's alkene groups generating SEs in close proximity of Cr atoms in the resist; Cr has a larger electron energy stopping power

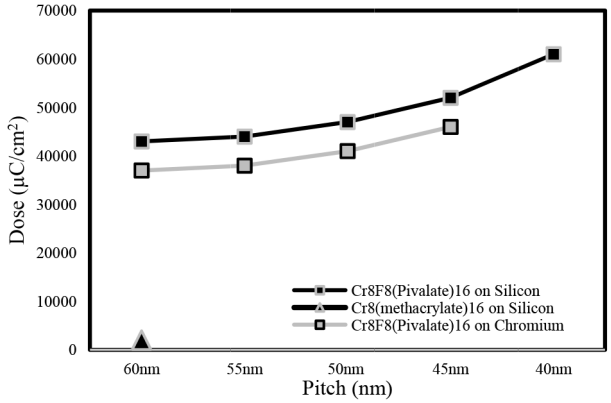

Figure 6. Electron exposure doses for the two resist materials on Si and Cr substrates.

than that of the C, O and H atoms in the organic molecule and therefore reduces the energy of the electron. As the energy reduction of the incident electron passes the threshold of which the probability of a secondary electron being created, they are free to collide with the Alkene groups in the Methacrylate molecule and this will allow more secondary electrons to be generated (their energy will be reduced more than the first generation) and this will create an avalanche effect until their associated energy is lower than 3.6 eV (which is the energy required to scission a C – C bond). As a result of the scattering angle the secondary electron penetrates through the Cr_8F_8(Methacrylate)$_{16}$ resist it exposes it laterally. This has the effect of reducing the resolution of the pitch.

The number of AEs generated is significant because there is a high probability of emitting low energy AEs from the 1S shell, since the lowest associated energy (5989 eV) for an incident electron shown in Figure 3b was 10 KeV. The Cr atom requires the largest associated incident electron energy to emit an AE in both resist systems because the excitation energy that is essential to ionize the electron from its ground state to a higher orbit is 5989 eV. EBL tools that operate at higher incident electron energies of the Cr electronic ground state are therefore able to take advantage of this process. It must be noted that EBL tools that use large acceleration voltages (50 KeV and above) will have a lower probability of emitting an AE because the scattering interaction is lower and this can be seen in Figure 3b. It is evident that incident electrons with low energies emit more AEs because the emitted AEs have low energy with respect to the energy of the incident electron, thereby increasing the statistical chance of creating further secondary and secondary Auger electrons (if the excitation energy of the secondary AEs is correct) upon each collision. Hence causing a chain reaction of cascading electrons in the immediate exposure area, leading to a significant reduction in exposure dose. It is clear that the dangling alkene groups of the methacrylate molecule are induced by all types of electrons (PEs, SEs and AEs) and generate significantly more AEs than that of the Cr_8F_8(Pivalate)$_{16}$ resist because they have an electron from the carbon atom that is free to be ionized from the ground state (this requires an excitation energy of 284.2 eV and the probability of generated SEs and emitted AEs having this discrete energy is high).

To build on the result and the explanation of Figure 3, Figure 4 shows the number of SEs and AEs that are generated in the Cr_8F_8(Methacrylate)$_{16}$ resist compared to the number generated in the Cr_8F_8(Pivalate)$_{16}$ resist, expressed as a ratio. This ratio was calculated to communicate the overall improvement in exposure performance of the alkene groups compared to the pivalates, which are expected to be less sensitive. It was found that the presence of the methacrylate molecule increased the sensitivity of the resist material, as predicted, thereby reducing the exposure doses required to produce a pattern. This is another way of expressing the results previously given in Figure 2 and 3, which show the same overall effect.

Compared to pivalate, methacrylate increases the number of generated SEs and AEs by a factor of 3.7 and 4.9, respectively, over the acceleration voltage range presented. The amplifications seen here increase the speed of the write times by increasing the solubility of the molecule upon the development process. Thus, to achieve the maximum resolution while avoiding overexposure, the exposure dose must be decreased to compensate for the extra concentration of electrons in the immediate exposure area. From this, the maximum write speed that can be theoretically achieved by Cr_8F_8(Methacrylate)$_{16}$ is approximately 23.6 times faster than Cr_8F_8(Pivalate)$_{16}$ at 100 KeV. This particular acceleration voltage is of interest as it was used to validate theoretical results with experimental results, which are presented next.

Figure 5 shows scanning electron microscope (SEM) micrographs of developed nanostructures written into Cr_8F_8(Pivalate)$_{16}$ and Cr_8F_8(Methacrylate)$_{16}$ resists. It is evident that Cr_8F_8(Methacrylate)$_{16}$ required an exposure dose lower than Cr_8F_8(Pivalate)$_{16}$ due to the introduction of the alkene groups. Even though the clearing dose of Cr_8F_8(Methacrylate)$_{16}$ is considerably reduced, Figure 5b clearly shows that the nanostructures could only be resolved at a pitch 60 nm (and no lower) as predicted by the results of the simulations (see Figure 3), while Cr_8F_8(Pivalate)$_{16}$ produced a pattern with a pitch as small as 40 nm. Figure 5c shows 15 nm features written into Cr_8F_8(Pivalate)$_{16}$ resist on 100 nm of Cr. Interestingly, only a 45 nm pitch could be achieved on those samples; this is because Cr, compared to Si only, leads to a higher number of BSEs emitted from the substrate layer back into the underside of the resist, contributing to the proximity effect. This is expected because the atomic number of Cr is 1.71 larger than that of Si; this is predicted by the results of the simulation.

Figure 6 shows how the exposure clearing doses vary with pitch of the pattern and confirms the role of the methacrylate molecules acting as SE and AE generators. The clearing dose in Cr_8F_8(Methacrylate)$_{16}$ is 22.6 lower than that in Cr_8F_8(Pivalate)$_{16}$, showing strong agreement with the factor of 23.6 predicted by simulation. The 4.3% simulation error is likely due to the Si substrate only having a thickness of 50 nm, whereas in the experiment, the substrate is 550 μm thick. The pattern exposure took place using incident electrons that had an acceleration voltage was 100 KeV; at this energy, the electrons can penetrate as deeply as 40 μm into the Si substrate and generate BSEs that get deposited into the underside of the resist, thus lowering both the exposure dose required and the patterning resolution.

It must be pointed out here again that the Monte Carlo simulator uses two models; the semi classical model accounts for electrons with

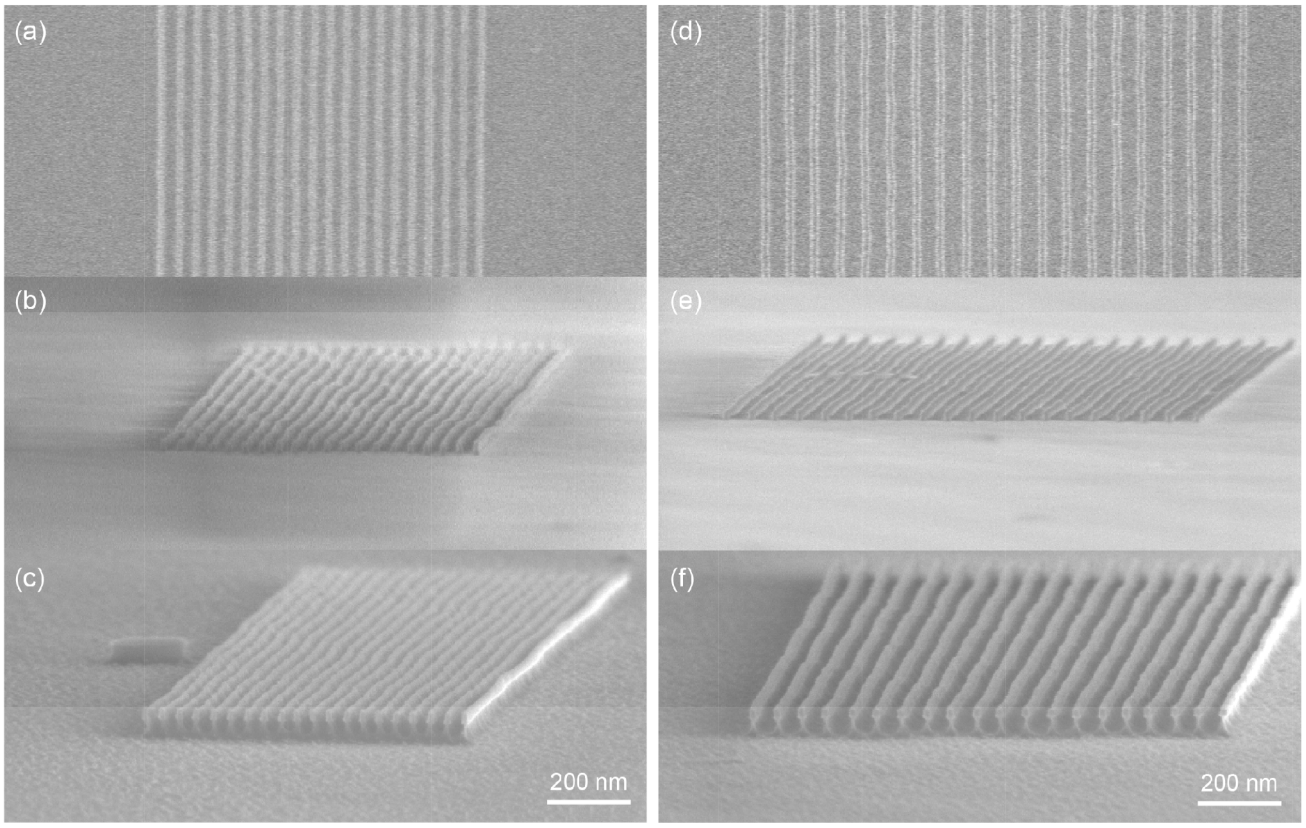

Figure 7. a) Top down view of 15 nm lines with a 40 nm pitch fabricated in $Cr_8F_8(Pivalate)_{16}$ resist on a Si. (b) Profile view of 15 nm lines on a 40 nm pitch fabricated in $Cr_8F_8(Pivalate)_{16}$ resist on Si. c) Profile view of $Cr_8F_8(Pivalate)_{16}$ resist on Si after a 20 sec pseudo Bosch dry etch process. d) Top down view of 15 nm lines on a 60 nm pitch fabricated in $Cr_8F_8(Methacrylate)_{16}$ resist on Si. (e) Profile view of 15 nm lines on a 60 nm pitch fabricated in $Cr_8F_8(Methacrylate)_{16}$ resist on Si. f) Profile view of $Cr_8F_8(Methacrylate)_{16}$ resist on Si substrate after a 20 sec pseudo Bosch dry etch process. Parameters: SF_6 and C_4F_8 gases were used with flow rates of 22 and 35 sccm, respectively; the deep reactive ion etching (DRIE) forward power was 20 W and the ICP forward power was 1200 W.

energies of 500 eV and above and the hard sphere method models quantum effects for electron energies of 100 eV and below. Clearly, some electrons may have energy in the 400 eV gap between the models, and are therefore unaccounted for. The simulator also does not account for x-rays generated by the electrons. These x- rays can cause bond scissions in the immediately exposure area and have the effect of lowering the exposure dose.

Figure 7a shows 15 nm nanostructures with a 40 nm pitch that have been patterned in the $Cr_8F_8(Pivalate)_{16}$ resist on a Si substrate. The resist exhibited extremely high dry etch selectivity when compared with Si. Since it is difficult to distinguish between the resist and Si in the micrographs, the Si was etched with conditions that created an undercutting effect, where the resist–Si interface can clearly be seen. Although this helps with characterization, it must be noted that this kind of undercut is an undesirable result in real FinFET fabrication.

The underlying Silicon was etched with a pseudo Bosch dry etch process that uses ICP of SF_6 and C_4F_8 gases. Before the etching process, Figure 7b shows that the resist produced a resolution of 15 nm while exhibiting a height of 25.4 nm. Figure 7c shows the resolution of the Si nanostructures after the etch was 11 nm, while exhibiting a height of 36.3 nm. The remaining resist thickness is measured to be 24.6 nm, which leads to an effective resist etch rate of 0.04 nm/sec over the 20 seconds of etch time, while the Si etch rate was 1.8 nm/sec. These measurements indicate a selectivity of 45:1. That is, the silicon etches 45 times faster than the resist. Figure 7d shows 15 nm nanostructures with a 60 nm pitch that have been patterned in the $Cr_8F_8(Methacrylate)_{16}$ resist on Si substrate; this was the best resolution that was obtained. Figure 7e shows 15 nm nanostructures with a 60 nm pitch while exhibiting a height of 22.5 nm. Figure 7f shows the width of Si nanostructures after the etch to be 16 nm, while exhibiting a height of 43 nm. The remaining resist thickness is measured to be 21.8 nm, which leads to the resist etch rate of 0.035 nm/sec, while the Si etch rate was 2.15 nm/sec. This indicates a selectivity of 61.4:1. This is approximately equivalent to the selectivity that is achieved with aluminum oxide masks[15], which were to this point the best masks available (it should be noted that the use of aluminum oxide masks requires more processing steps and has increased costs compared to this process). It is evident that the additives of the methyl methacrylate do not affect the etching performance of this material; clearly the chromium oxide does not react with the SF_6 or C_4F_8 gases. As the gases come into contact with the resist, there is no chemical reactivity, thus the resist keeps its structural integrity and yields a large selectivity. This is significant because other resists such as PMMA, ZEP520A and HSQ have etch selectivities of only 2:1, 2.89:1 and 4.16:1, respectively[16]. That is, the highest dry etch resistance among these commonly used resists is only a little over 4 times that of Si. The new material reported here outperforms each of these materials by a factor of at least ~14.75.

At first glance, it appears that the Si etching process for the $Cr_8F_8(Pivalate)_{16}$ resist exhibits a poorer etch selectivity when compared to the $Cr_8F_8(Methacrylate)_{16}$ resist. This is not the case, because the pitch was 20 nm smaller and therefore the etch efficiency was decreased, which inherently decreased the etch rate of the underlying substrate and produced a smaller etch depth, leading to a decrease in the selectivity. An experiment in which the pitch is extended to 100

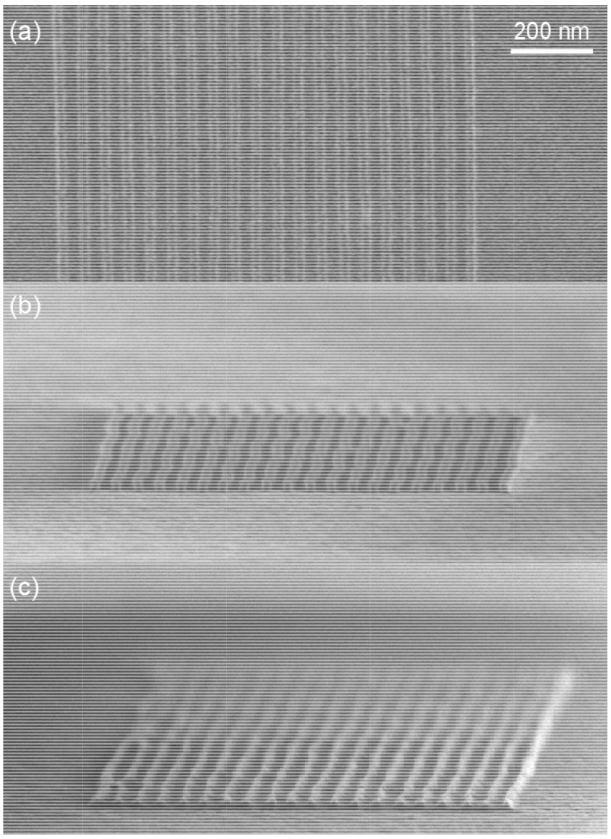

Figure 8. a) Top down view of 15 nm lines with a 50 nm pitch fabricated in $Cr_8F_8(Pivalate)_{16}$ resist on a 100 nm layer of Cr on Si substrate. (b) Profile view of the nanostructures shown in (a). (c) Profile view of the nanostructures following a 20 sec pseudo Bosch dry etch process, showing fins with a 8 nm width. Parameters: Cl_2 and O_2 gases were used with flow rates of 100 and 3 sccm, respectively; the DRIE forward power was 100 W and the ICP forward power was 1000 W.

or 200 nm is expected to show equal or near-equal etch selectivity, once the small pitch effect is mitigated[4].

Figure 8a shows 15 nm lines on a 50 nm pitch that have been patterned in the $Cr_8F_8(Pivalate)_{16}$ resist on a 100 nm Cr layer that was deposited on Si substrate. The underlying Cr layer was etched with a dry etch process that uses an ICP of Cl_2 and O_2 gases. Before the etching process, Figure 8b shows that the resist yielded line widths of 15 nm while exhibiting a height of 26.7 nm. Figure 8c shows the width of the Cr nanostructures after the etch was 15 nm, while exhibiting a height of 20 nm. The profile of these Cr nanostructures are triangular in shape, likely due to over etching. The resist has been totally eroded away, which leads to a calculated resist etch rate of 1.33 nm/sec, while the Cr etch rate was 1.0 nm/sec. This yields a selectivity of 0.75:1, meaning that Cr etches 0.25 times slower than $Cr_8F_8(Pivalate)_{16}$ resist with this etch. This is not a surprising result because after electron beam exposure, the $Cr_8F_8(Pivalate)_{16}$ resist is converted into a chromium oxide material and the chemical reaction rate of the Cl_2 gas with the chromium oxide is expected to be high.

4. Conclusion

In summary, two metal organic negative tone electron beam resist have been investigated. It was shown by the Monte Carlo simulations that the $Cr_8F_8(Methacrylate)_{16}$ resist material generated a significant number of secondary and Auger electrons within the resist when compared to the $Cr_8F_8(Pivalate)_{16}$ resist, due to the presence of alkene groups. It was found that $Cr_8F_8(Pivalate)_{16}$ resist produced very high-resolution nanostructures (15 nm in width) while exhibiting a pitch of 40 nm. This high resolution came at the expense of sensitivity, however; the clearing dose of this resist material was 61000 μC/cm^2 at 40 nm pitch and 43000 μC/cm^2 at 60 nm pitch. It was shown that the low sensitivity was dramatically improved by replacing the pivalate component with a methacrylate molecule; the clearing dose of this altered resist material was 1900μC/cm^2 at 60 nm pitch (40 nm pitch was not achievable with this material). Substituting methacrylate for pivalate, therefore, resulted in a 22.6 fold increase in resist sensitivity. This experimental result was in strong agreement with simulations, which predicted an increase by a factor of 23.6. Preliminary studies showed that both resists have a remarkable pseudo Bosch dry etch resistance compared to silicon (selectivity was calculated to be 61:1 for the methacrylate resist and 45:1 for the pivalate resist). The high etch resistance is due to the presence of the d-block metal (Cr) in the initial resist, which ultimately yields a chromium oxide hard mask following exposure to an electron beam and subsequent development in solvent.

5. Acknowledgements

We acknowledge the EPSRC(UK) for funding (grant EP/R023158/1). The University of Manchester also supported this work. The authors gratefully acknowledge critical support and infrastructure provided for this work by the Kavli Nanoscience Institute at Caltech.

6. References

[1] van Dodewaard, A. J., Roes, R. F. M., Kwinten, J. A. J., van Delft, F. C. M J. M., v n Run, A. J., van Langen-Suurling, A. K. and Romijn, J., "Comparison of Negative tone resists NEB22 and UVN30 in E-beam lithography", *Microelectronic Engineering 53* (1 – 4) 61 – 464 (2000).

[2] Masnyj, Z., Mangat, P., Ainley, E., Nordquist, K. and Resnick, D., "Evaluation of negative DUV UVN30 for electron beam exposure of NGL masks", **Proc. SPIE 3997**, Emerging technologies IV, 0277-786x, (2000).

[3] Klein, C., Loeschner H. and Platzgummer, E., "50KeV electron multibeam mask writer for the 11nm HP node: first results of the proof of concept tool (eMET POC)", **Proc SPIE 8323**, Alternative Lithographic Technologies IV, 83230G (2012).

[4] Lewis, S. M., Fernandez, A., DeRose, G. A., Hunt, M. S., Whitehead, G. F. S., Lagzda, A., Alty, H. R., Ferrando-Soria, J., Varey, S., Kostopoulos, A. K., Schedin, F., Muryn, C. A., Timco, G. A., Scherer, A., Yeates, S. G. and Winpenny, . E. P., "Us of Supramolecular Assemblies as Lithographic Resists", *Angew. Chem. Int. Ed., 56,* (24), 6749-6752 (2017).

[5] Noto, V. D., Boeer, A. B., Lavina, S., Muryn, C. A., Bauer, M., Timco, G. A., Negro, E., Rancan, M., Winpenny, R. E. P. and Gross, S., "Functional chromium wheel-based hybrid organic-inorganic materials for dielectric applications", *Adv. Funct. Mater. 2009,* 19, 3226–3236, (2009).

[6] Laye, R. H., Larsen, F. K., Overgaard, J, Muryn, C. A, McInnes, E. J. L., Rentschler, E., Sanchez, V., Teat, S. J., Güdel, H. U., Waldmann, O., Timco, G. A. and Winpenny, R. E. P., "A family of heterometallic wheels containing potentially fourteen hundred siblings", *Chem. Commun.,* 1125–1127 (2005).

[7] Lewis, S. M. and DeRose, G. A., Frontiers of Nanoscience, Materials and Processes for Next Generation Lithography, Elsevier, 421, 12, (2016).

[8] Joy, D. C., *Monte Carlo Modeling for Electron Microscopy and Microanalysis*. New York: Oxford University Press, 1995.

[9] Sakurai, J. J. and Tuan, San Fu, *Modern Quantum Mechanics*. Menlo Park, California; Wokingham: Benjamin- Cummings, 1985.

[10] Wolff, P.A., "Theory of Secondary Electron Cascade in Metals", *Physical Review,* 95 (1) (1954)

[11] Shimizu, R. and Ze-Jun, D., "Monte Carlo modelling of electron-solid interactions", *Rep. Prog. Phys.* 487- 531(1992).

[12] Zianni, X., Velessiotis, D., Glezos, N. and Trohidou, K. N., "Application of the partial wave expansion method in 3-D low energy electron beam lithography simulation", *Microelectronic Engineering*, 57-58: 297-302 (2001).

[13] You, D. S., Li, H. M. and Ding, Z. J., "Monte Carlo simulation of Auger electron emission from thin film on substrate", *J. Electron Spectrosc. Relat. Phenom.,* 222, 156–161 (2018).

[14] Casnati, E., Tartari, A. and Baraldi, C., "An empirical approach to K-shell ionisation cross section by electrons", *J. Phys. B: At. Mol. Phys. 15,* 155 (1982).

[15] Henry, D., S. Walavalkar, S., Homyk, A. and Scherer, A., "Alumina etch masks for fabrication of high-aspect-ratio silicon micropillars and nanopillars", *Nanotechnology, 20,* (25), 255305 (2009).

[16] A. Goodyear, M. Boettcher, I. Stolberg and M. Cooke, "Direct comparison of the performance of commonly used e- beam resists during nanoscale plasma etching of Si, SiO_2 and Cr", **Proc. SPIE 9428,** 94280V, (2015).

BACUS N • E • W • S

Sponsorship Opportunities

Sign up now for the best sponsorship opportunities

Photomask Technology + EUV Lithography 2019

Contact: Melissa Farlow,
Tel: +1 360 685 5596; **melissaf@spie.org**

Advanced Lithography 2019

Contact: Teresa Roles-Meier,
Tel: +1 360 685 5445; **teresar@spie.org**

Advertise in the BACUS News!

The BACUS Newsletter is the premier publication serving the photomask industry. For information on how to advertise, contact:

Melissa Farlow,
Tel: +1 360 685 5596
melissaf@spie.org

BACUS Corporate Members

Acuphase Inc.
American Coating Technologies LLC
AMETEK Precitech, Inc.
Berliner Glas KGaA Herbert Kubatz GmbH & Co.
FUJIFILM Electronic Materials U.S.A., Inc.
Gudeng Precision Industrial Co., Ltd.
Halocarbon Products
HamaTech APE GmbH & Co. KG
Hitachi High Technologies America, Inc.
JEOL USA Inc.
Mentor Graphics Corp.
Molecular Imprints, Inc.
Panavision Federal Systems, LLC
Profilocolore Srl
Raytheon ELCAN Optical Technologies
XYALIS

Industry Briefs

Semiconductor Equipment Sales Forecast: $62B in 2018 a New Record

Releasing its Year-End Total Equipment Forecast at the annual SEMICON Japan exposition, SEMI reported that worldwide sales of new semiconductor manufacturing equipment are projected to increase 9.7 percent to $62.1 billion in 2018, exceeding the historic high of $56.6 billion set last year. The equipment market is expected to contract 4.0 percent in 2019.

The SEMI Year-end Forecast predicts wafer processing equipment will rise 10.2 percent in 2018 to $50.2 billion. The other front-end segment – consisting of fab facilities equipment, wafer manufacturing, and mask/reticle equipment – is expected to increase 0.9 percent to $2.5 billion this year. The assembly and packaging equipment segment is projected to grow 1.9 percent to $4.0 billion in 2018, while semiconductor test equipment is forecast to increase 15.6 percent to $5.4 billion this year.

https://electroiq.com/2018/12/semiconductor-equipment-sales-forecast-62b-in-2018-a-new-record/

Global Semiconductor Sales Up 9.8% Year-to-Year in November

The Semiconductor Industry Association (SIA), representing U.S. leadership in semiconductor manufacturing, design, and research, today announced worldwide sales of semiconductors reached $41.4 billion for the month of November 2018, an increase of 9.8 percent from the November 2017 total of $37.7 billion and 1.1 percent less than the October 2018 total of $41.8 billion. Monthly sales are compiled by the World Semiconductor Trade Statistics (WSTS) organization and represent a three-month moving average.

“The global semiconductor industry continues to post solid year-to-year sales increases, and year-to-date revenue through November has surpassed annual sales from all of 2017, but growth has slowed somewhat in recent months,” said John Neuffer, SIA president and CEO. “Year-to-year sales increased in November across all major regional markets, with the China market standing out with growth of 17 percent. Double-digit annual growth is expected for 2018 once December’s sales are tallied, with more modest growth projected for 2019.”

https://electroiq.com/2019/01/global-semiconductor-sales-up-9-8-year-to-year-in-november/

ASML Developing Next-Gen EUV Lithography

ASML vice president Anthony Yen says that ASML has begun development of the extreme ultraviolet lithography machine his company believes will be needed to continue shrinking the features of silicon chips once today’s systems reach their limits.

The ASML 5000 will rely on a number of evolutionary improvements over the 3400 series, which customers such as Intel, Samsung, and TSMC are using now. The most noticeable will be an increase in the machine’s numerical aperture from today’s 0.33 to 0.55, Yen told engineers at the IEEE International Electron Device Meeting this week in San Francisco. Numerical aperture is a dimensionless quantity related to how tightly light can be focused. A higher numerical aperture means better resolution. Changing the numerical aperture in the EUV machine will require a larger, more perfectly polished set of imaging mirrors.

https://spectrum.ieee.org/nanoclast/semiconductors/devices/asml-developing-next-gen-euv-lithography

Join the premier professional organization for mask makers and mask users!

About the BACUS Group

Founded in 1980 by a group of chrome blank users wanting a single voice to interact with suppliers, BACUS has grown to become the largest and most widely known forum for the exchange of technical information of interest to photomask and reticle makers. BACUS joined SPIE in January of 1991 to expand the exchange of information with mask makers around the world.

The group sponsors an informative monthly meeting and newsletter, BACUS News. The BACUS annual Photomask Technology Symposium covers photomask technology, photomask processes, lithography, materials and resists, phase shift masks, inspection and repair, metrology, and quality and manufacturing management.

Individual Membership Benefits include:

- Subscription to BACUS News (monthly)
- Eligibility to hold office on BACUS Steering Committee

spie.org/bacushome

Corporate Membership Benefits include:

- 3-10 Voting Members in the SPIE General Membership, depending on tier level
- Subscription to BACUS News (monthly)
- One online SPIE Journal Subscription
- Listed as a Corporate Member in the BACUS Monthly Newsletter

spie.org/bacushome

CALENDAR

2019

Photomask Japan
16-18 April 2019
PACIFICO Yokohama
Yokohama, Japan
photomask-japan.org

SPIE Advanced Lithography
24-28 February 2019
San Jose Marriott and
San Jose Convention Center
San Jose, California, USA

The 35th European Mask and Lithography Conference, EMLC 2019
17-19 June 2019
Hilton Hotel Dresden
Dresden, Germany

SPIE Photomask Technology + EUV Lithography
15-19 September 2019
Monterey Conference Center and
Monterey Marriott
Monterey, California, USA

SPIE is the international society for optics and photonics, an educational not-for-profit organization founded in 1955 to advance light-based science, engineering, and technology. The Society serves nearly 264,000 constituents from 166 countries, offering conferences and their published proceedings, continuing education, books, journals, and the SPIE Digital Library in support of interdisciplinary information exchange, professional networking, and patent precedent. SPIE provided more than $4 million in support of education and outreach programs in 2018. spie.org

SPIE.
International Headquarters
P.O. Box 10, Bellingham, WA 98227-0010 USA
Tel: +1 360 676 3290
Fax: +1 360 647 1445
help@spie.org • www.SPIE.org

Shipping Address
1000 20th St., Bellingham, WA 98225-6705 USA

Managed by SPIE Europe
2 Alexandra Gate, Ffordd Pengam, Cardiff,
CF24 2SA, UK
Tel: +44 29 2089 4747
Fax: +44 29 2089 4750
spieeurope@spieeurope.org • www.spieeurope.org

You are invited to submit events of interest for this calendar. Please send to lindad@spie.org; alternatively, email or fax to SPIE.